Physical and mechanical metallurgy of high purity Nb for accelerator cavities

T. R. Bieler,[1] N. T. Wright,[2] F. Pourboghrat,[2] C. Compton,[3] K. T. Hartwig,[4] D. Baars,[1] A. Zamiri,[2] S. Chandrasekaran,[2] P. Darbandi,[1,2] H. Jiang,[1] E. Skoug,[1] S. Balachandran,[4] G. E. Ice,[5] and W. Liu[6]

[1]*Chemical Engineering and Materials Science, Michigan State University, East Lansing, Michigan 48824-1226, USA*
[2]*Mechanical Engineering, Michigan State University, East Lansing, Michigan 48824-1226, USA*
[3]*National Superconducting Cyclotron Laboratory, Michigan State University, East Lansing, Michigan 48824-1321, USA*
[4]*Mechanical Engineering, Texas A&M University, College Station, Texas 77843, USA*
[5]*Division of Materials Science & Technology, Oak Ridge National Laboratory, Oak Ridge, Tennessee 37831, USA*
[6]*Advanced Photon Source, Argonne National Laboratory, Argonne, Illinois 60439, USA*

(Received 29 November 2009; published 15 March 2010)

In the past decade, high Q values have been achieved in high purity Nb superconducting radio frequency (SRF) cavities. Fundamental understanding of the physical metallurgy of Nb that enables these achievements is beginning to reveal what challenges remain to establish reproducible and cost-effective production of high performance SRF cavities. Recent studies of dislocation substructure development and effects of recrystallization arising from welding and heat treatments and their correlations with cavity performance are considered. With better fundamental understanding of the effects of dislocation substructure evolution and recrystallization on electron and phonon conduction, as well as the interior and surface states, it will be possible to design optimal processing paths for cost-effective performance using approaches such as hydroforming, which minimizes or eliminates welds in a cavity.

DOI: 10.1103/PhysRevSTAB.13.031002 PACS numbers: 81.05.Bx, 74.70.Ad, 61.72.Ff, 66.70.Df

I. INTRODUCTION

The continuing efforts to improve cavity performance to attain a high electric field and quality (efficiency) factor, Q, have shown that the theoretical limit for the maximum field of about 42 MV/m is within reach [1]. As this limit is approached, identification of factors accounting for sub-theoretical performance becomes increasingly important in order to reduce variability in performance. A number of hypothetical reasons have been put forward, many of which are linked to the metallurgical state of the Nb, particularly in welds. As there are many possible variables, discussion will become less speculative if fundamental understanding of the physical metallurgy processes that occur along the fabrication path is clarified. This paper provides an overview of what is known about the evolution of metallurgical state, and identifies areas needing further examination; a condensed version of this paper is in [2].

The primary focus will be on factors that affect formability of Nb and cavity performance based upon classical [3–5] mechanical and physical metallurgical knowledge. These topics are insufficient to identify all that accounts for variability in performance, as there are additional factors related to electromagnetic and superconducting states in the few nanometers near the surface of the interior, which are discussed in other papers [6–8]. This paper will focus on the evolution of defect structures, primarily dislocation substructure, and how it affects cavity manufacturing and performance. The basic crystal structure is discussed first, followed by physical metallurgical changes that occur with forming, welding, heat-treating, etching, and baking.

II. BCC DISLOCATION CHARACTERISTICS

Pure Nb is a body centered cubic (BCC) metal similar to steel in structure only, as steels contain other elements (always C, S, P, Mn, sometimes Al, Si, Ti, V, Cr, Ni, Nb, Mo). Much of the metallurgy of steel is focused on exploiting the phase transformation from face centered cubic (FCC) to BCC (Fig. 1) that occurs around 700–900°C, and controlling the distribution of C in interstitial positions and carbide precipitates. Interstitial carbon and small precipitates have a large influence on the generation of mobile defects such as vacancies and dislocations (terminated half planes of atoms), which determine the strength and ductility of the alloy. In FCC metals (e.g. Al, Cu, Pb, some stainless steels), dislocation and mechanical twinning processes are confined to {111} planes with dislocation motion in the ⟨110⟩ and ⟨112⟩ twinning directions.[1] Conversely, dislocations in the BCC structure move in ⟨111⟩ directions on {110}, {112}, and {123} planes. In FCC metals, there are 12 slip systems of three slip directions on four slip planes. In BCC metals, there are six {110} slip planes on which there are two slip directions, which also provide 12 slip systems. Because BCC metals are also able to slip along the same four ⟨111⟩ directions on {112}, and {123} planes,

[1]The symbols {} and ⟨⟩ around "Miller indices" are used to describe families of similar (symmetric) crystallographic planes and directions, respectively, in terms of the cubic lattice. The symbols () and [] refer to specific members of the family of planes and directions, respectively, arising from any permutation of positive and negative integers in the family. For example, four ⟨111⟩ directions, six {110} planes, 12 {112} planes, and 24 {123} planes are present in any cubic structure.

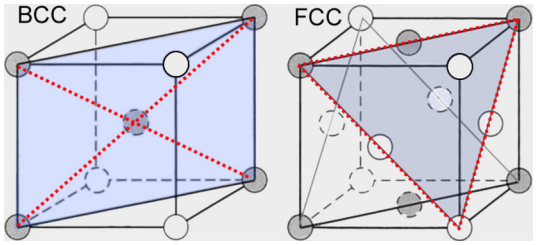

FIG. 1. (Color) Comparison between BCC and FCC crystal structures. Examples of slip planes are shaded, and slip directions identified with dotted lines.

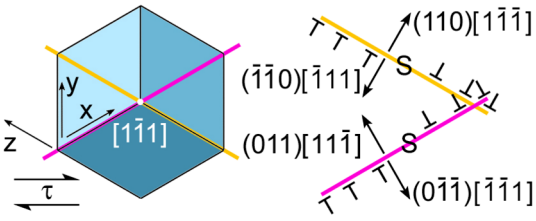

FIG. 2. (Color) Two {110} slip planes with a common [111] axis perpendicular to the page are illustrated on a cubic unit cell. Motion of dislocations from sources S arise due to an imposed shear stress τ that activates two slip systems. The plane normal and slip directions are described with Miller indices such that the scalar product is zero; each system can be equivalently described in two ways using opposite signs (bars over numbers).

BCC metals have as many as 48 distinct slip systems available; 12 on the six {110} planes, 12 on the 12 {112} planes, and 24 on the 24 {123} planes. While slip on {123} planes is observed in Nb at large strains that occur in rolling [9], it appears to be less active in forming operations of recrystallized material, where strains are smaller. There are two equivalent descriptions for each system illustrated in Fig. 2, where each slip system is defined with a plane and shear direction; the same sense of shear can be accomplished by dislocations on either side of the slip plane, moving in opposite directions. Dislocation sources often generate matched sets moving in opposite directions [10]. Operation of several slip systems is usually required to change the shape of an object such as a grain in a polycrystal, leading to intersections (Fig. 2). When dislocations interact, they become curved, which alters the structure of the dislocation core into a mixture of edge and screw components, as illustrated in Fig. 3.

In the BCC structure, dislocations reside in deep energy wells, and their motion requires significantly greater mechanical force than in FCC metals. Thermal vibration provides a large fraction of the energy needed to move dislocations in BCC metals. This makes all BCC metals very strong at cryogenic temperatures, as illustrated in Fig. 4 [11], which shows how the flow stress for Nb drops by an order of magnitude as the temperature changes from near-0 to ambient. The shear stress τ and the shear strain

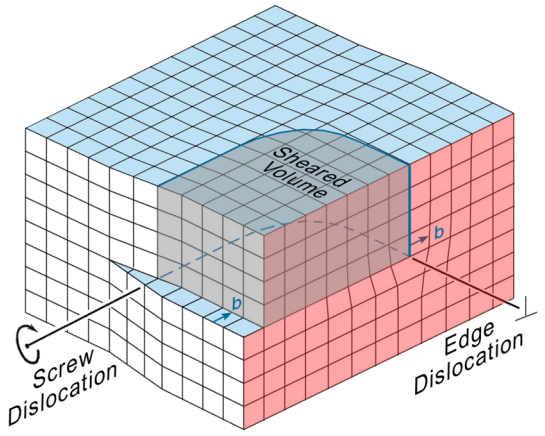

FIG. 3. (Color) Curved dislocations have edge and screw components.

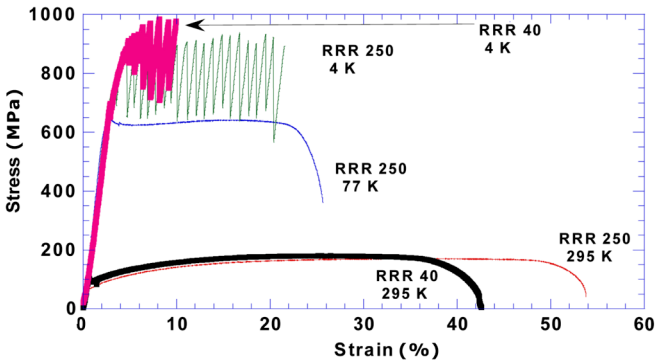

FIG. 4. (Color) Temperature dependence of Nb flow stress, used with permission from AIP [11].

rate $\dot{\gamma}$ on a slip plane are related by the Orowan equation $\dot{\gamma} = \rho b \bar{v}$, where ρ is the dislocation density, $\bar{v}$ is the average velocity, and b the Burgers vector (unit of motion of a dislocation, i.e., the atomic spacing on the slip plane). The velocity v is a strong function of stress, given by $v = v_o(\tau/\tau_o)^m$, where v_o and τ_o are a reference velocity and stress, and m is a large positive exponent, (e.g. ~25). Observations of dislocations in BCC metals show mostly the screw orientation, which implies that the edge dislocation has higher mobility than a screw dislocation [4]. At an imposed strain rate, a yield drop is a natural consequence of dislocation multiplication from an initially low density, such that the average velocity decreases, and with it, the stress. The yield stress in BCC metals is also highly sensitive to interstitial atom content, as interstitial atoms will diffuse into dislocation cores to lock them, even at room temperature. These interstitials raise the mechanical energy needed to force dislocations to break away from the solute atoms that pin them, leading to an initial yield drop once the stress is sufficiently high. This sudden yield drop is commonly observed in plain carbon steels and lower purity Nb.

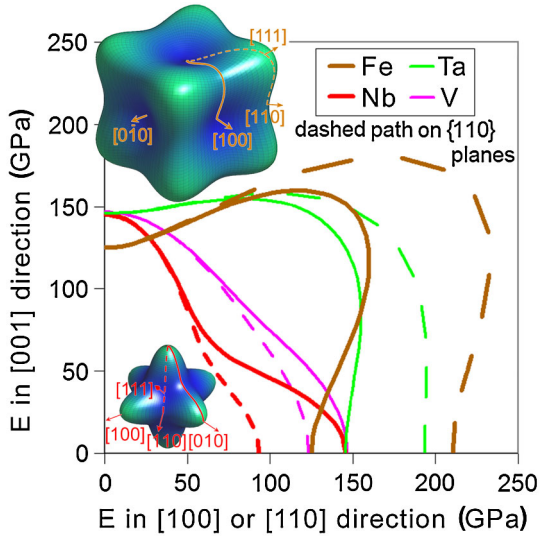

FIG. 5. (Color) The elastic anisotropy of BCC metals is plotted on {100} and {110} planes showing maximum and minimum values of Young's (tensile) modulus, E (the vector from the origin to the curve gives the direction and magnitude). The maximum stiffness in Fe is along ⟨111⟩, which is the most compliant in Nb. Nb is the most compliant of BCC metals [12].

Pure Nb is a much simpler metal than steel because it lacks the complexities of the FCC-BCC transformation coupled with precipitation of second phases that enable a wide range of microstructures and properties. In contrast to Fe, only the dislocation substructure, the grain shape, size, orientation, and misorientation distribution can be modified in pure Nb. Furthermore, the elastic anisotropy of Nb is the opposite of Fe, as illustrated in Fig. 5 [12], which affects the core structure of dislocations in Fe and Nb. In Fe, the direction of ⟨111⟩ dislocation slip is in the stiffest direction in the crystal, whereas in Nb, it is the most compliant direction (low spring constant). Nb is the most compliant of all the BCC metals, which may arise from Nb being the only group 5 metal with an extra *d* shell electron instead of a filled *s* shell. These differences make extrapolations of properties of steel to Nb rather dubious.

As dislocations on a slip plane impose an elastic repulsive force on neighboring dislocations, a pileup of same signed dislocations generated by strain against a grain boundary (which controls the yield stress) leads to internal elastic back stresses that resist formation of more dislocations. The stress imposed on a barrier by a pileup of dislocations (e.g. a grain boundary or an entanglement) is proportional to $n\boldsymbol{\tau}$, where n is the number of dislocations in a pileup and $\boldsymbol{\tau}$ is the stress needed to initiate slip [10]. Consequently, to achieve the same internal stress in Nb as in Fe, Nb would require more than 3 times the number of dislocations, as $E_{111}(\mathrm{Fe})/E_{111}(\mathrm{Nb}) = 3.3$. Because the interaction forces between dislocations in Nb are much smaller, dislocation entanglements lead to much smaller internal stresses in Nb, and hence, dislocations are much more stable in Nb.

Figure 6 shows stress-strain curves for nine single-crystal orientations [13] on specimens cut from a 2.8 mm thick slice from an as-cast ingot produced by Ningxia (China), with a 18 mm long, 4 mm wide gage section. Table I shows how these specimens were cut to favor different slip systems or combinations of slip systems. Slip will occur when the resolved shear stress from an imposed stress (quantified using the Schmid factor) exceeds the critical resolved shear stress. The critical resolved shear stress (CRSS) for {112}⟨111⟩ slip is about 5% lower than for slip on {110}⟨111⟩ systems, but when both of these systems are nearly equally favored with the same slip direction, their interactions raise the CRSS by about 6%–8%. The work hardening rate is strongly depen-

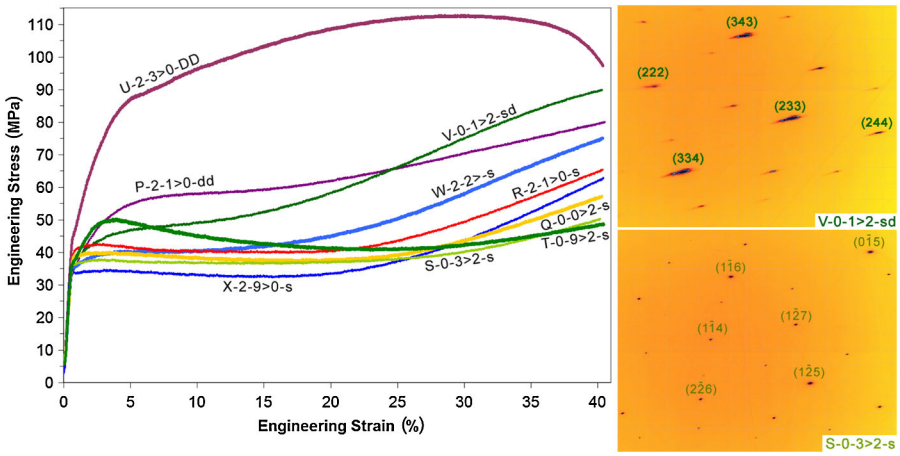

FIG. 6. (Color) Stress-strain curves for nine single crystals described in Table I oriented to investigate slip system interactions; some have a single slip direction (S) for much of the deformation (curves that are more nearly flat). Five specimens show softening, and three others have multiple slip directions activated (SD, DD) that cause stress increases (work hardening) from dislocation intersections, entanglements, and lattice rotations made evident by streaked diffraction patterns. The diffraction patterns from white synchrotron radiation represent orientations from a ~1 μm diameter column of atoms about 100 μm deep.

TABLE I. Intended slip system activation in single-crystal tensile specimens from Ningxia ingot slice.

Name	Initial order of Schmid factors on slip systems	τ_{CRSS}, MPa, initial slip behavior
U3	{112}, {112} 3.3% lower τ in *different direction*,	16.2 extremely high hardening
2–3 > 0-DD	{110} 5% lower same, {110} 8% lower different	All four have low Schmid factors
P3	{112}, {112} 1% lower τ in *different direction*,	16.5 high hardening
2–1 > 0-dd	{110} 4.5% lower same, {110} 4% lower different	Four slip systems with high Schmid factor
V3	{110}, {112} 1.2% lower τ in same direction	16.6 moderate hardening
0–1 > 2-sd	{110} 1.8%, {112} 4% lower different directions	Four slip systems with high Schmid factor
W3	{112}, {110} 2.3% lower τ in same direction	16.3 slight hardening
2–2 > 0-s	{112} and {110} 9% lower in different direction	
X3	{112}, {110} 8.5% lower τ in same direction	16.7 upper yield point, slight softening
2–9 > 0-s	{110} 22% lower in same direction	
R3	{112}, {110} 1.4% lower τ in same direction	19.0 initial hardening, then softening
2–1 > 0-s	{110} 30% lower in different direction	
Q2	{110}, {112} 0.35% lower τ in same direction	18.6 slight softening
0–0 > 2-s	{110} 17% lower in different direction	
S3	{110}, {112} 3.0% lower τ in same direction	17.3 slight softening
0–3 > 2-s	{110} 15% lower in different direction	
T3	{110}, {112} 9.3% lower τ in same direction	17.6 high initial hardening, ends up softest
0–9 > 2-s	{110} 17% lower in different direction	

dent on slip system interactions; when slip is favored on two planes with the same slip *direction*, the work hardening (rate of stress increase) is much smaller than when two slip systems with different slip directions are favored.

These specimens were examined using the 3D x-ray diffraction microscope at the Advanced Photon Source (APL) at Argonne National Laboratory to obtain information about dislocation substructure. Specimens showed streaked or spread diffraction patterns in most cases, as illustrated in selected areas of diffraction patterns for two specimens. The streaks indicate the presence of orientation gradients, and by implication, *geometrically necessary dislocations* (GND [14]). In one case, the diffraction pattern did not show streaks, which probably resulted from dislocations being able to pass completely through the specimen without generating entanglements (investigations on these specimens are on-going). Four of the nine samples exhibiting flow softening (stress decreases after a peak stress), which may arise from large changes in mobile dislocation density, or other complex dislocation behavior discussed by other researchers [15,16]. Initial dislocation density present in the ingot (discussed next) may account for variability in hardening rates, as well as a higher critical resolved shear stress than observed in other experimental work [17].

III. INGOT PRODUCTION

As high purity Nb is produced using multiple electron beam remelts of a Nb ingot, the solidified lower part of the ingot collects droplets of molten Nb, and hence the top of the ingot is at the melting temperature. This is done slowly to permit evaporation of most of the impurity elements (Ta is not effectively removed this way, as it has a low vapor pressure). The slow production rate and the lack of impurity atoms enables grain growth, so that large grains such as those shown in Fig. 7 are present in ingots. However, the water cooled mold causes a large spatial temperature gradient, which causes strains associated with thermal contraction. Figure 8 shows a region in a large grain ingot with significant populations of tangled dislocations (white) that are between cells of low dislocation density material (dark) [18]. It is not yet known if this heterogeneous dislocation structure is typical, but such dislocation structures cause several degrees of orientation spread within a grain, which has been observed consistently in inverse pole figures obtained from orientation imaging microscopy [OIM™, or electron backscattered diffraction pattern (EBSP) analysis] data sets (Fig. 9). This orientation spread implies that there are more geometrically necessary dislocations than are observed in recrystallized grains (discussed later).

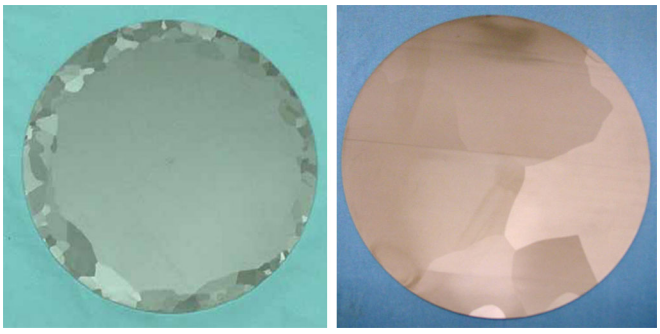

FIG. 7. (Color) Cross sections of two ingots from different manufacturers illustrating large grains, and differences in morphology arising from different processing conditions.

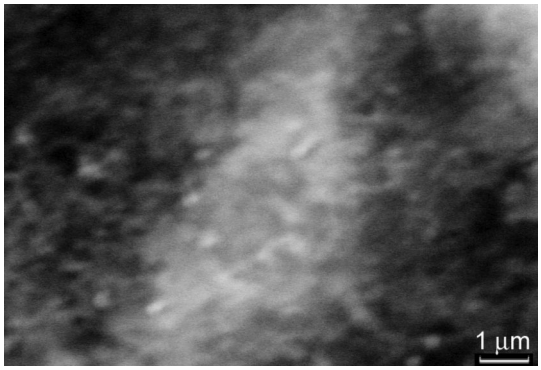

FIG. 8. Electron channeling contrast image of dislocation structure in an as-received ingot.

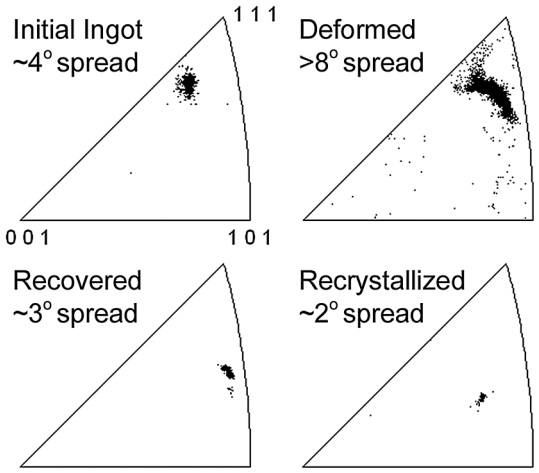

FIG. 9. Representative discrete inverse pole figures from OIM^{TM} measurements from different specimens. The spread of crystal orientations is greatest after deformation, and significantly lower after heat treatments to cause recovery or recrystallization.

IV. SHEET METAL PRODUCTION

Rolling accomplishes two goals: to break down the initially large grains to create a uniform fine grain size, and to change the shape from a slab or billet into sheet. Ingots are sectioned into billets (which may only contain a few grain orientations) and cold forged to a suitable shape that is then rolled using multiple reductions according to typically proprietary schedules, and annealed at strategic times during this process [19]. As high purity Nb is not a mass produced product, the billet is commonly small enough to allow rolling in multiple directions, which can improve the formability of products made from rolled sheet.

The rolling process causes different deformation modes on the surface and center; the shear on the surface activates slip systems that rotate crystals differently from the plane-strain compression in the center, as illustrated in Fig. 10(a) [5]. These differences in strain-path typically cause {111} to be approximately parallel to the sheet normal direction

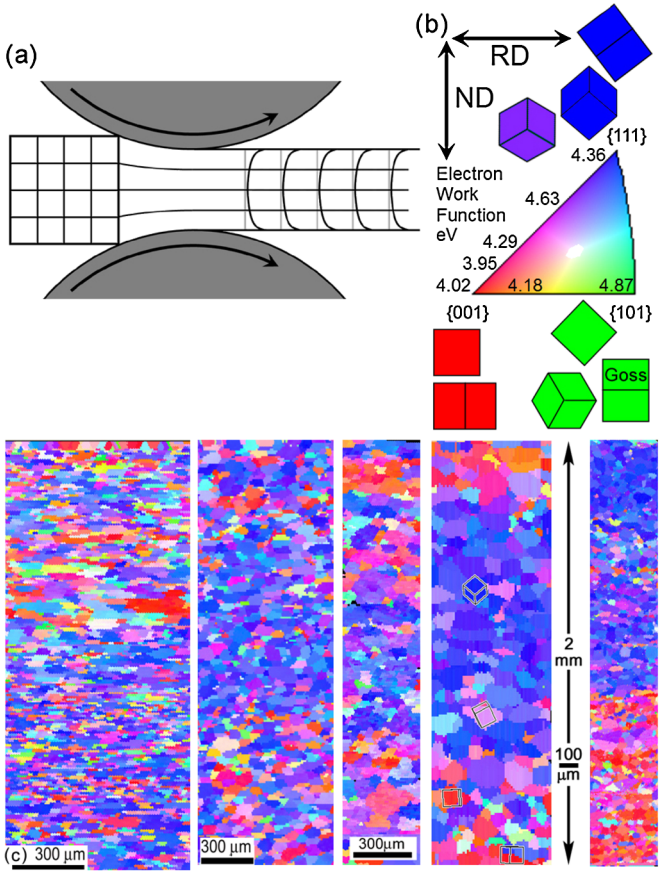

FIG. 10. (Color) Schematic diagram (a) illustrates how the strain path differs between the surface and center of rolled sheet, resulting in different distributions of grain orientations based upon the color convention illustrated (b, where the electron work function values are also indicated for different surface normal directions [21]). Five examples of full thickness orientation maps (c) from high purity Nb commercially rolled to ~2 mm thick [20] show a trend of preferred {100} orientations near the surface and {111} orientations in the interior. The microstructure and texture gradients vary widely from sample to sample. These orientation maps are with respect to the vertical sheet normal direction (ND).

(ND) in the interior, and grains on the surface to have {100} parallel to the ND, for example, the {100}⟨011⟩[2] rotated cube orientation. More commonly, a range of orientations with a common crystal direction normal to the sheet are found, such as {100} ∥ ND [i.e. red orientations in Figs. 10(b) and 10(c) [20]]. Similarly, {111} ∥ ND preferred orientations are also common (named the γ fiber;

[2]The {plane}⟨direction⟩ nomenclature identifies an orientation about which there is commonly a spread of about 10°. The notation {100}⟨011⟩ indicates that {100} planes are approximately parallel to the sheet (i.e. the plane normal is perpendicular), and ⟨011⟩ directions are aligned preferentially with the rolling direction. It is usually written so that the scalar product would be zero, consistent with the orthogonal relationship between the sheet normal and the rolling direction.

blue orientations). These orientation map colors are based upon a convention that has been established for visually assessing the texture and microstructure of rolled cubic metals, with {111} blue, {110} green, and {100} red, as viewed in the sheet normal direction Fig. 10(b). This is the default color code in EBSP data acquisition programs if the measured surface is the sheet normal (but if the cross section is measured, the orientation data must be rotated to be consistent with this convention). Rolling generally causes rotations that increase the fraction of the γ fiber, but the rate at which this occurs depends on the starting orientations. For example, the rotated cube orientation is stable up to a 70% thickness reduction, after which slip commences on {123} planes that alters the texture to generate more of the γ fiber [9,21]. The γ-fiber orientations are also stable. Other orientations are less stable, so crystals naturally rotate toward orientations between {001} and {111}, and hence, orientations between these two terminal stable orientations dominate (pink and purple orientations). Thus, orientations with {110} ∥ ND (green orientations) cannot be achieved with rolling.

Because the surface and center strain paths have different stress states and strain paths, they cause different rotations and different levels of stored strain energy (dislocation density), so subsequent recrystallization is rarely uniform. Often, the surface shows larger grain sizes than in the interior. To achieve a sufficiently uniform small grain size (to meet specifications), producers have often given a small reduction prior to the final anneal that selectively puts more plastic work into the surface grains. While this leads to a more consistent grain size, it also increases the fraction of {100} grains on the surface. From about ten characterizations of different batches of rolled material from different suppliers, the same combination of grain orientation distribution (texture) and grain size has never been observed twice, even among pieces from the same batch of material. One of the examples in Fig. 10 even shows the upper half with {111} and the lower half with {100} planes preferred in the sheet normal direction. This implies that a method to reproducibly obtain the same microstructure from a billet has not been achieved by commercial suppliers, and this can cause variability in forming half cells.

Some of the variability in cavity performance may be traceable to the variability of grain orientations on the surface, which etch at different rates, and have different work functions (the work function varies with surface normal direction as indicated on the inverse pole figure triangle in Fig. 10 [22]).

V. INFLUENCE OF MICROSTRUCTURE AND TEXTURE ON FORMABILITY

Processes have been developed in many metal and alloy systems to optimize uniform in-plane formability of sheet metal by controlling texture (distribution of grain orientations) and microstructure. Perhaps the most finely tuned example is the control of microstructure and texture that is necessary in the aluminum beverage can industry. It is well established that a small grain size favors more uniform and larger strains, and also minimizes surface roughness (orange peel) that arises from heterogeneous strain in different grains. Minimizing surface roughness minimizes perturbations that can initiate damage or fatigue cracks, and as important, the fine grain size improves the application and appearance of paint.

The two orientation types commonly found on the surface and center of Nb sheet have very different mechanical and formability properties. On the surface, the red {100} ∥ ND is relatively soft in tension tests, resulting from all four of the ⟨111⟩ slip directions having a ~35° inclination from the sheet that causes high resolved shear stresses on many slip systems. In-plane tension will *activate* from 4–8 slip systems in most {100} ∥ ND orientations that cause the greatest amount of change in thickness possible per unit of strain, leading to preferential thinning. A dominant red orientation will lead to preferred deformation, while other minority orientations deform much less, leading to self-amplifying strain localization and considerable surface roughness [23,24]. In contrast, the blue {111} ∥ ND orientation γ fiber typically has three *activated* ⟨111⟩ slip vectors that are inclined 20° from the plane, and with the 4th ⟨111⟩ direction perpendicular to the plane, it has no resolved shear stress acting on it. Because of the smaller inclination angle, more shear strain is required to attain a given thickness reduction, so a larger applied stress is needed to accomplish the same strain, making it a harder orientation. These orientations resist thinning because a large strain causes the least amount of change in thickness possible, and hence less surface roughness. This is also a stable orientation because if two slip systems operate preferentially, they will rotate the crystal in a direction where the third one becomes favored, causing a counter rotation. Because the blue orientation is hard, minority orientations will strain in a manner that is constrained by the majority blue orientations, resulting in uniform deformation. With biaxial forming, the slip behavior is more complex, but the {111} orientation is still more desirable for uniform large strain formability.

In processing for optimal formability, strategic changes in rolling direction combined with heat treatment can bias crystal rotations toward a desired {111} orientation, but when the final thickness is reached, strain can no longer be used to change the texture. This limitation on the available strain to control microstructure and texture can be overcome to obtain highly desirable textures with fine grain sizes using the equal channel angle extrusion (ECAE) processes prior to rolling (Fig. 11 [25]). In a study that examined different processing paths, different billets of material were pushed through the 90° die several times with different 90° or 180° rotation sequences, which alter

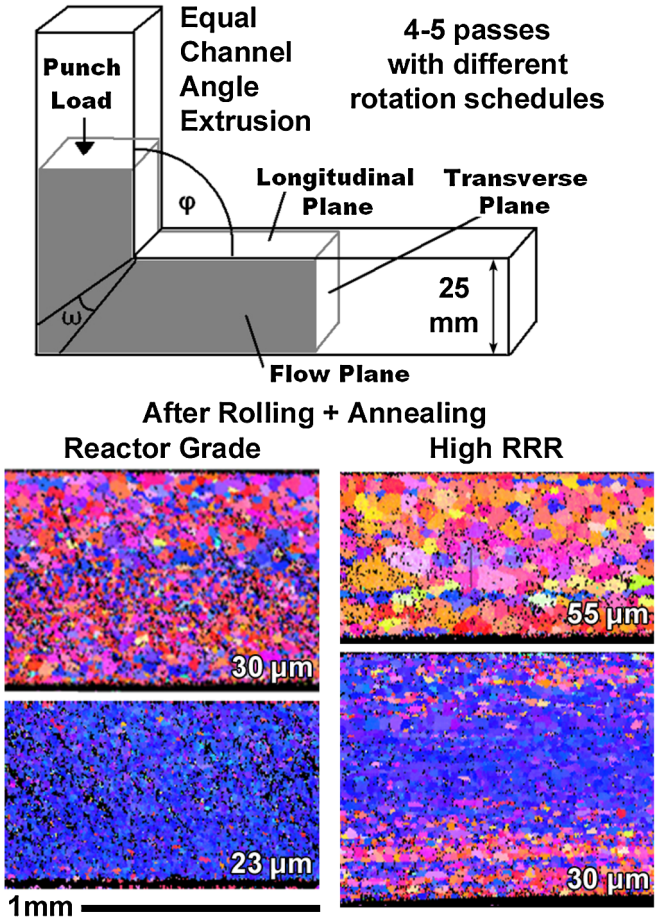

FIG. 11. (Color) Very different kinds of rolled sheet microstructures and texture gradients can be obtained for samples preprocessed with ECAE; the color scale is the same as Fig. 7 [25], and the white labels indicate a characteristic grain size.

the texture evolution, but do not change the billet shape. Every preconditioning path tried led to a nearly homogeneous texture and grain size after annealing. Using these preconditioned billets, subsequent rolling led to more consistent microstructures and textures than usually observed in commercial sheet, which would lead to more consistent formability. Four examples (of about 20 examined) of annealed rolled sheet are illustrated; each had different ECAE preprocessing schedules, but they had the same rolling and final anneal schedule [the annealing temperature was 1000°C for reactor grade (99.98%), and 700°C for >99.99% high-RRR Nb (residual resistance ratio of the resistance at 298 K to that at 4.2 K)]. The resulting microstructures, textures, and even final thicknesses differ significantly even though they had the same annealing, rolling, and final annealing history after the ECAE preprocessing step. It is noteworthy that >95% gamma fiber was achieved with one process history in the reactor grade material using a particular process path that was not tried for the high-RRR material, but the path closest to this successful path used in the high-RRR material is shown. Because solute atoms control the migration rates of grain boundaries, what is achieved in one composition may or may not be achievable in another.

An interesting outcome from orientation analysis is the complete absence of {011} texture in any of the commercial Nb sheet, or any of the 20 ECAE preprocessed rolled sheets (Figs. 10 and 11). This {011} orientation is attractive for superconducting radio frequency (SRF) cavities because it has the highest electron work function of any orientation [Fig. 10(b)]. In grain oriented silicon steels, a very high fraction of the {011}⟨100⟩ Goss orientation can be obtained with a strategic combination of strain and recrystallization annealing [26–28]. In Fe, the highest magnetic permeability and minimal hysteretic loss occur in the ⟨001⟩ direction, so steels with strong Goss texture are used in transformers. Goss grains form predominantly from shear bands in deformed {111}⟨112⟩ orientations, which naturally arise during rolling. Silicon steels are similar to high purity Nb, as Si is in solution, Si stabilizes the BCC structure, and they have very low interstitial (O, C) content, but Si steels also have second phase particles that are important for controlling grain size. The fact that Goss grains do not form in Nb when it has so many other similarities with silicon steel indicates that the presence of small particles in Si steels and/or the opposite elastic anisotropy and its effect on dislocation energy dramatically affect how recrystallization proceeds.

Computational plasticity modeling strategies can be used to simulate forming processes, and computational optimization methods can be used to identify desirable processing strategies. Using the measured texture as an input, these orientations can be computationally deformed in a manner that ensures compatibility in strains (so that no voids occur) on an average (statistical) basis [29,30]. It is also possible to computationally deform particular microstructures to assess heterogeneous deformation characteristics [31,32]. As each grain has different combinations of active slip systems, the amount of slip on each system varies *within* grains so that compatible deformation occurs with neighboring grains. These modeling processes are complex, and must consider how accumulation of disloca-

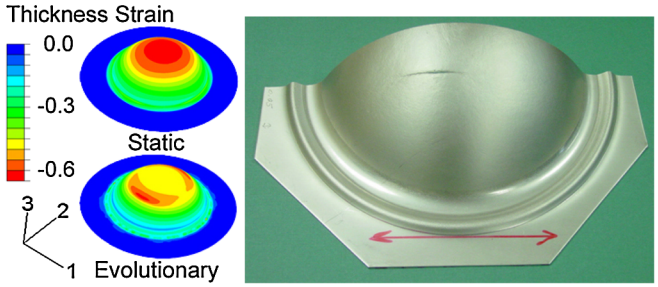

FIG. 12. (Color) Simulations of biaxial bulging using two variants of crystal plasticity finite element models with different assumptions [33,34]; the better one used an evolving yield surface based upon texture evolution.

tions causes rotation, hardens the microstructure, and increases the stress needed to accomplish the next increment of deformation, such that the flow properties evolve. Figure 12 shows two outcomes starting with the same set of initial grain orientations, but using different ways of tracking hardening behavior; the more sophisticated model is able to predict locations where failure is more likely [33,34].

Slicing ingots to form cavities

There is growing interest in bypassing the cost and uncertainties associated with rolled material by slicing disks from ingots and forming cavities from the multicrystal slices [19]. When pressed in molds, the deformation is often much more irregular than from fine grain sheet metal, requiring extra pressing operations and jigs to obtain circular mating surfaces needed to weld two half cells together. Thicknesses are much more irregular, even within the same grain orientation, because the direction of hoop stress varies spatially with respect to the grain orientation, such that different slip systems will be activated in different parts of the same large grain. Grain boundaries impose barriers to slip, so that less strain occurs along grain boundaries, leading to easily detected ridges along grain boundaries (easily felt with fingers). These irregularities may be worth tolerating for benefits that come with reduced waste material and reduced cost of rolling and heat treating, but this also introduces an element of variability that must be either tolerated or overcome with strategic processing of ingots to obtain consistent grain orientations, or strategic choices of which pieces (and orientations) should be welded together.

VI. RECOVERY AND RECRYSTALLIZATION

In both deformation processing to make sheet and in forming of the cavity, heat treatments are required to restore ductility, or drive out hydrogen, or modify the interior surface of the cavity. These processes remove dislocations generated by plastic deformation, but this process is extremely sensitive to details of deformation history, preferred grain orientations, microstructure/grain size, temperature, time, heating rate, and thermal gradient history, making this process challenging to control. Compared to steels, niobium recrystallizes in a more random manner [35], making preferred textures more difficult to obtain. Having fewer processing variables available (compared to steel) also limits the ways that recrystallization can be strategically used to obtain desirable grain orientations and microstructures.

Heat treating causes changes in the microstructure by the mechanisms of recovery, recrystallization, and grain growth, which are briefly described in Figs. 13 and 14 [35]. During plastic deformation, entangled dislocations cause dislocation multiplication processes [3–5]. Formation of a mobile dislocation defect results in separation of intact planes of atoms to become two terminated half planes of opposite sign which are separated by shear displacements. Dislocation intersections also cause generation of excess vacancies. Neighboring half planes with opposite signs have attractive stress fields, so with diffusion processes at elevated temperature and a much higher vacancy concentration than equilibrium allow most of these terminated half planes to find neighboring half planes with the opposite sign. As they join to recover a whole plane, two dislocations are removed (i.e., recovery). Such dislocation reactions eliminate *statistically stored dislocations*, so the remaining *geometrically necessary dislocations* [which cause lattice curvature, Fig. 13(b)] reorganize with the aid of diffusion to form planar low angle subgrain boundaries. This process occurs three dimensionally to form polygonized subgrain boundaries consisting of equally spaced dislocations, Fig. 13(c). These low angle boundaries can move under the influence of stress, but they are very stable due to their low energy. They can most easily be removed by sweeping a high angle grain boundary through the material.

The minimum temperature for recovery occurs at a lower temperature than recrystallization and grain growth, so partial recovery events precede recrystallization. The recrystallization temperature depends on many factors, such as strain history, dislocation density, rate of heating (full recovery can prevent recrystallization), and purity. Impurities segregate preferentially to grain boundaries

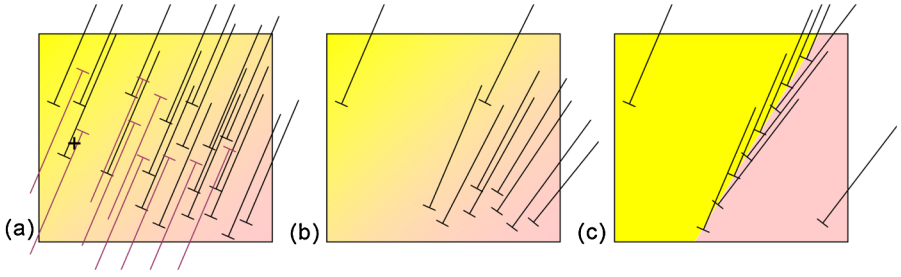

FIG. 13. (Color) Schematic diagram of recovery: (a) after plastic deformation, statistically stored dislocations climb and glide to find annihilation partners (e.g. location marked with +), leaving only (b) geometrically necessary dislocations which can (c) arrange themselves into low energy low angle boundaries with time.

and dislocation substructures, and can stabilize boundaries and dislocation structures, so that a higher temperature is required to facilitate their motion, and this is why reactor grade Nb has a higher recrystallization temperature than high-RRR Nb.

There are many kinds of recrystallization mechanisms that depend on specific details of different materials and compositions [36]. For high purity niobium, where hot deformation is not needed to form complex shapes, deformation plus annealing to get recrystallization causes *primary* recrystallization. The driving force for primary recrystallization is removal of dislocations and subgrain boundaries, which is accomplished by sweeping a high angle boundary through the deformed crystal. As a grain boundary moves through a region with subgrains, atoms from grains with subgrains jump into perfect lattice sites, resulting in elimination of subgrains and most dislocations (there are always some dislocations present to satisfy the need for entropy). Because the strain energy of dislocations is so small in Nb, the density of dislocations in recrystallized grains is likely to be greater than in steels or most other metals. Figure 14 shows two ways this can occur. In Fig. 14(a), subgrains that recover in a shear band develop a mobile high angle boundary that grows into lesser deformed adjacent material. Figure 14(b) illustrates a different scenario, where the smaller subgrain size in one grain has higher defect density, so the neighboring grain boundary bulges into this grain (known as strain induced grain boundary migration).

Once primary recrystallization occurs to the point where a high angle grain boundary has swept through deformed material, the driving force for continued grain growth is to reduce the interfacial energy of grain boundaries, leading to larger grains. Hence, the same volume element may have several boundaries pass through it. In Si steels that form the Goss orientation, a secondary recrystallization takes place; a Goss oriented grain becomes larger than neighboring grains, and thus gains a growth advantage and consumes the surrounding grains. Secondary recrystallization can be controlled using second phase particles which pin grain boundaries in a way that facilitates development of a minority large grain that can gain the growth advantage. The lack of particles in Nb may preclude the ability to grow a Goss orientation even if it once existed in suitably oriented shear bands [37]. It is of great technological value to control which grain boundaries move in order to obtain desirable recrystallized orientations, but in high purity Nb, grain boundary mobility is especially hard to control as even very small changes in composition can dramatically alter how alloy atoms segregate preferentially to some boundaries [38].

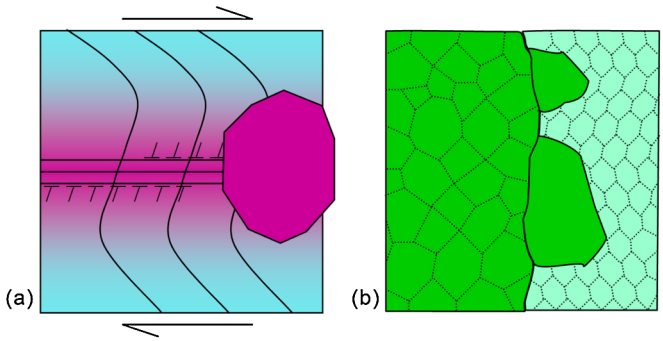

FIG. 14. (Color) Schematic diagram of two forms of recrystallization: (a) subgrains within locally rotated shear bands nucleate to grow into surrounding lesser deformed material; (b) grain with larger subgrains (left) grows into grain with smaller subgrains (right).

VII. WELDING

Welding is a necessary part of fabricating accelerator hardware, although there are methods to reduce the number of welds or even make weldless cavities with spinning or hydroforming processes [39]. In current practice, half cells are e-beam welded together. As welding progresses, solidification, recrystallization, and recovery occur near the weld, dramatically altering the parent microstructure in the heat affected and fusion zones [40]. Figure 15(a) shows a polycrystal weld in undeformed material that was exposed to air prematurely, so that differential oxidation rates re-

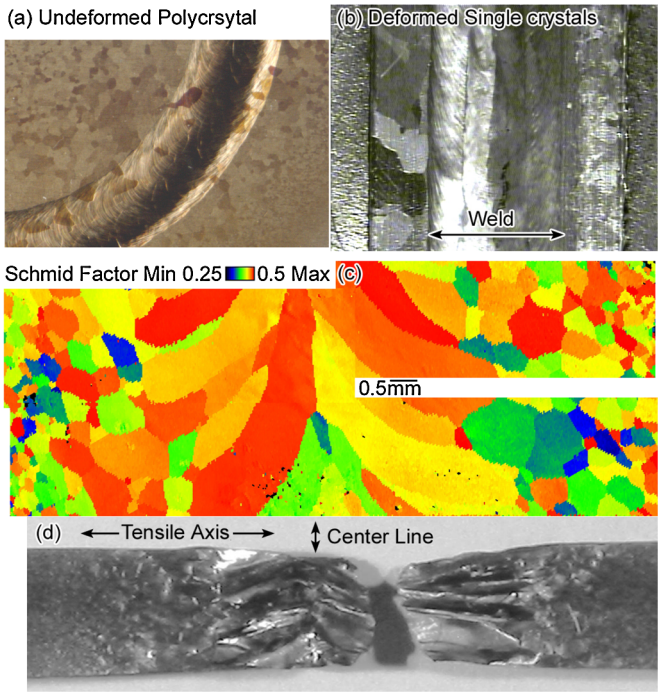

FIG. 15. (Color) (a) Test weld on an undeformed polycrystal plate exposed to air while cooling shows differential oxidation that reveals the microstructure present in the material. (b) Weld between two deformed single crystals has a single orientation on either side in the fusion zone, but recrystallization occurs in the HAZ. Grains with high Schmid factors from OIM^{TM} map (c) deform preferentially during a tensile experiment (d) [40].

vealed the grain structure. The fastest oxidation rates occurred on grains with {111} plane normals. Deformed single crystals recrystallize in the heat affected zone (HAZ), but the fusion part of the weld is often a bicrystal with a boundary along its centerline [Fig. 15(b)]. Grains within the fusion zone of polycrystals are large and have varied orientations [Figs. 15(a) and 15(c)], which give the weld very different properties from the parent material. The HAZ adjacent to the fusion zone of the weld has a dramatic gradient of grain sizes, and the heating allows adsorbed interstitial atoms to diffuse beneath the surface, altering purity in complex ways that depend on temperature and time. Adjacent to the weld, recrystallization and dramatic grain growth occur, and farther away, some grain growth and recovery occurs to varying extents. The large grain sizes lead to a slightly lower yield stress and much more nonuniform strain, with elongations about half to 2/3 of the parent material. As the two parts to be welded are held in fixtures, cooling causes thermal contraction and localized strain in the weld and HAZ. In instrumented cavity tests, hot spots have most often been found in the HAZ of the equator weld, making the weld a suspicious source of defects that degrade cavity performance [39].

Figure 16 shows a detailed investigation of effects of welding, recrystallization, and recovery. Tensile specimens of single crystals were deformed to about 40% strain, similar to the stretching that occurs at the iris of an elliptical cavity, cut in half, and two different halves were welded together in a manner similar to that used for welding cavities from deformed large grain slices. The two ends of the tensile specimens were clamped, providing a heat sink, as well as constraint during cooling that caused thermal contraction strains. From the weld to the shoulder of the specimen, the thermal history varied considerably, as indicated schematically in Fig. 17 [41]. Figure 16 shows an orientation map of a welded tensile specimen from one end to the other, and beneath it, a kernel average misorientation (KAM) map, which identifies the magnitude of local lattice curvature among the tens of pixels immediately surrounding each pixel of orientation information. The physical metallurgy state of each zone of the specimen is described.

Weld (fusion zone).—In the solidified region grains have clearly grown into the fusion zone from the adjacent HAZ, and are nearly defect free. In particular, the small green orientation just to the right of the weld in Fig. 16 is a recovered grain orientation (with the same orientation as the deformed orientation). Analysis with OIM™ and synchrotron x rays showed that the recovered grain had orientation gradients, but the same orientation in the weld had no gradients [35].

HAZ.—There is evidence in Fig. 16 that the red and blue orientations on the right side (C), and all the nonblue orientations on the left side (F) are recrystallized grains in the HAZ. Even within this recrystallized zone, there are orientation gradients evident along grain boundaries, e.g., surrounding the light purple grain on side F, and between the red and blue grains at the triple point with the green grain on side C. There are regions with lattice curvature within recrystallized grains, particularly on each side of the light purple grain in the middle of side F, which may have

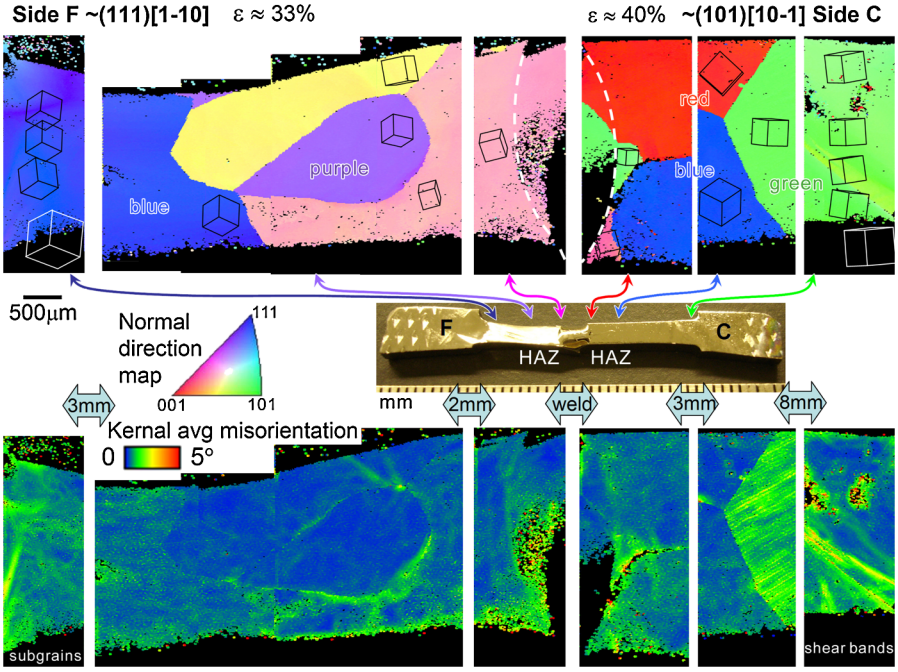

FIG. 16. (Color) Two deformed single-crystal tensile specimens with initial orientations shown with white prisms were deformed to nominally 40% strain, cut in half, and welded together to simulate welding of single-crystal cavities [35]. The specimen recrystallized in the heat affected zone (HAZ), but the temperature gradient halted the recrystallization front about 4–5 mm from the weld.

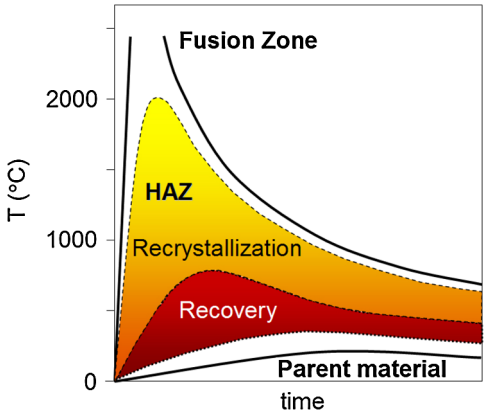

FIG. 17. (Color) Schematic diagram of heating and cooling history in different zones of a weld [41].

developed from straining during cooling. Details regarding the recrystallized grain orientation relationships and possible mechanisms are discussed in [35].

Recovered regions of the HAZ have the same orientation as the deformed grain, and they contain more orientation gradients and, hence, GNDs [scattered green (gray) colors in the KAM plots] than the recrystallized grains. There is evidence of subgrain boundaries in the recovered blue grain just to the left of the three recrystallized grains on the left side (F) and planar slip traces in the green grain just to the right of the red and blue recrystallized grains on side (C). These orientation gradients oscillate, as the orientation maps do not show long range color gradients.

Slightly heated regions near shoulder.—Shear bands are evident as bands of green-yellow color inclined to the stress axis on KAM maps on side C in Fig. 16. The left side (F) shows cells on the KAM map where dislocation entanglements caused local regions of higher lattice curvature.

VIII. SURFACE PREPARATION

After welding, the interior surface is chemically removed to eliminate a "damaged layer" of about 100–200 μm [40]. Etching clearly removes any deformation features arising from handling, but it also removes {100} orientations that have a lower work function, which often predominate on the surface (Fig. 10). An 800°C vacuum heat treatment is often used to drive out hydrogen, and this causes a mixture of recovery and recrystallization that depends on the strain and location with respect to welds, so dislocation density is clearly reduced, but not in a uniform manner. While grain boundaries have been shown to trap magnetic flux vortices that cause local heating [6–8], it is not yet clear if dislocation substructure is also able to do this. Correlations between hot spots in cavities and higher geometrically necessary dislocation content have been identified in the context of experiments investigating the effects of the final 120°C bake that improves cavity performance [42]. There are also correlations between hot spots and etch pits in the HAZ, which are often indications of dislocations [43]. The nature and mechanisms of dislocation rearrangement during the 120°C bake remains an open question.

IX. DISLOCATION SUBSTRUCTURE AND THERMAL CONDUCTIVITY

Thermal conductivity (k) is also sensitive to dislocation content. Normally conducting electrons conduct heat, but their number decreases with temperature, so consequently, k also decreases as more electrons become superconducting with decreasing temperature, as illustrated in Fig. 18. It is well known that lattice defects interfere with normal electron conduction (i.e. resistivity), which is a component of k. Electrical resistivity is one of the earliest methods used to measure dislocation density, and this method has been extensively used to characterize recovery and recrystallization [3]. High Q values have been obtained because the high purity increases k by removing impurity atoms that disturb electron flow.

With decreasing temperature, the fraction of normally conducting electrons decreases, and the dominant mechanism of heat conduction changes from electron to phonon conduction at about 3 K. Dislocations can also affect phonon transport [44]. When unpinned segments of dislocations are aligned with the heat flow direction, a passing phonon can be dissipated by causing the dislocation to vibrate within its energy well, and thus reduce energy transport to the He bath surrounding the cavity. These considerations indicate that thermal conductivity is tied to the RRR, which is illustrated in Fig. 18 [45]. The black

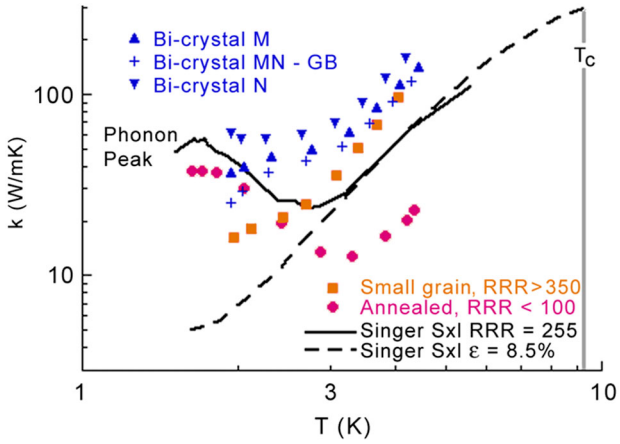

FIG. 18. (Color) Measurement of thermal conductivity, k: the two curves from Singer [45] show how strain in a single crystal removes the phonon peak. An as-received polycrystal (orange symbols) showed no phonon peak, but after a 1400°C anneal, the phonon peak returned, but due to a low quality vacuum, the thermal conductivity at higher T dropped extensively. A bicrystal specimen (blue symbols) shows modest effects of grain orientation and boundary on k.

lines show how the peak in phonon conductivity between 1 and 3 K disappeared after a strain of 8.5%, indicating that dislocations greatly reduced phonon conduction, as the thermal conductivity follows the trend arising from the decreasing population of normal conducting electrons. The red symbols illustrate a polycrystal specimen that was annealed in a vacuum furnace with a low quality vacuum, such that the electronic thermal conductivity was degraded, yet the annealing increased the conductivity in the phonon conduction region below 3 K. Thus, the measured RRR may reflect both purity *and* dislocation content. In recent bicrystal experiments, differences in k with respect to crystal orientation, as well as resistance at a grain boundary, are resolved in the measurements indicated by blue symbols. As the RRR is unknown, it is not clear whether the lack of grain boundaries, purity, or dislocation content was responsible for the higher normally conducting k, and the differences arising from the grain boundary or the grain orientations. Recent work with deformed and annealed single crystals is even more dramatic; k at the phonon peak is an order of magnitude larger. Clearly, dislocation content is a significant contributor to the value of k in cavities, and the presence of residual dislocations is generally undesirable.

X. SUMMARY

This overview of the mechanical and physical metallurgy associated with the production of SRF cavities clearly shows that dislocations are an omnipresent facilitator for and detractor of the performance of cavities. There is only a small amount of knowledge about the underlying physics of dislocations on functional performance. Processing paths can be optimized to obtain desirable microstructures for forming, but there is also evidence that dislocations affect thermal conductivity and rf currents on the interior surface. Two exemplary forming histories illustrate where deeper understanding of the metallurgical state is needed: Cost saving can be achieved by slicing ingots to avoid the cost of making rolled sheet, but it is also likely to bring variability arising from large crystal orientations and welds. Cost savings may also be possible if strategic deformation processing is used to optimize polycrystalline Nb for hydroforming in order to remove the variability arising from welds. Perhaps a recrystallized single-crystal or large grain cavity with few dislocations aligned with the direction of heat flow may lead to optimal and reproducible performance of a cavity. Whether this can be done without compromising other practical design constraints (such as strength or dimensional stability) presents an optimization challenge.

ACKNOWLEDGMENTS

This work was supported by DOE (ILC), under Contract No. DE-FG02-06ER41433, and Fermi National Laboratory. Use of the Advanced Photon Source was supported by the U.S. Department of Energy, Office of Science, Office of Basic Energy Sciences, under Contract No. W-31-109-Eng-38. G. E. I. was supported by the Division of Materials Sciences and Engineering, U.S. DOE.

[1] G. Ciovati, J. Appl. Phys. **96**, 1591 (2004).
[2] T. R. Bieler, Advances in Material Studies for SRF, SRF2009, Berlin, Germany, SRF2009 WEB Proceedings, paper TUOAAU03, pp. 102–108, ISSN 1868-5781.
[3] R. Abbaschian, L. Abbaschian, and R. E. Reed-Hill, *Physical Metallurgy Principles* (CL-Engineering, Stamford, CT, 2009), 4th ed.
[4] D. Hull and D. J. Bacon, *Introduction to Dislocations* (Butterworth-Heinemann, Oxford, 2001), 4th ed.
[5] G. E. Dieter, *Mechanical Metallurgy* (McGraw-Hill Science Engineering, New York, 1986), 3rd ed.
[6] A. Romenenko, Ph.D. dissertation, Cornell University, 2009.
[7] A. Gurevich, Appl. Phys. Lett. **88**, 012511 (2006).
[8] G. Ciovati and A. Gurevich, Phys. Rev. ST Accel. Beams **11**, 122001 (2008).
[9] D. Raabe and K. Lücke, Z. Metallkd. **85**, 302 (1994).
[10] D. Hull and D. J. Bacon, *Introduction to Dislocations* (Butterworth-Heinemann, Oxford, 1984), 3rd ed.
[11] R. P. Walsh, Ke Han, V. J. Toplosky, and R. R. Mitchell, in *Proceedings of the International Cryogenic Materials Conference–ICMC*, edited by B. Balachandran *et al.*, AIP Proc. No. 48 (AIP, New York, 2002), pp. 186—193.
[12] G. Simmons and H. Wang, *Single Crystal Elastic Constants and Calculated Aggregated Properties: A Handbook* (MIT Press, Cambridge, MA, 1971), 2nd ed.
[13] D. Baars, T. Bieler, P. Darbandi, F. Pourboghrat, and C. Compton, Microstructure Studies on Niobium, SRF2009, Berlin, Germany, SRF2009 WEB Proceedings, paper TUOBAU05, pp. 144–48, ISSN 1868-5781.
[14] G. E. Ice and R. Barabash, *White Beam Microdiffraction and Dislocations Gradients in Dislocation in Solids*, edited by F. R. N. Nabarro and J. P. Hirth (Elsevier, New York, 2007), Chap. 79, pp. 502–601.
[15] A. Seeger and U. Holzwarth, Philos. Mag. **86**, 3861 (2006).
[16] R. Gröger, A. G. Bailey, and V. Vitek, Acta Mater. **56**, 5412 (2008).
[17] M. A. Siddiq, Doctorate dissertation, Universität Stuttgart, 2006.
[18] D. Baars, T. R. Bieler, A. Zamiri, F. Pourboghrat, and C. Compton, SRF 2007 Beijing, China, TUP05, http://web5.pku.edu.cn/srf2007/.
[19] 19. P. Kneisel, G. R. Myneni, G. Ciovati, J. Sekutowicz, and T. Carneiro, AIP Conf. Proc. **927**, 84 (2007).
[20] H. Jiang, D. Baars, A. Zamiri, C. Antonie, P. Bauer, T. R. Bieler, F. Pourboghrat, C. Compton, and T. L. Grimm, IEEE Trans. Appl. Supercond. **17**, 1291 (2007).
[21] H. Jiang, T. R. Bieler, C. Compton, and T. L. Grimm, Physica (Amsterdam) **441C**, 118 (2006).

[22] R. P. Leblanc, B. C. Vanbrugg, and F. E. Girouard, Can. J. Phys. **52**, 1589 (1974).
[23] A. R. Zamiri, F. Pourboghrat, and T. R. Bieler, J. Appl. Phys. **104**, 084904 (2008).
[24] D. Raabe, M. Sachtleber, H. Weiland, G. Scheele, and Z. Zhao, Acta Mater. **51**, 1539 (2003).
[25] K. T. Hartwig, J. Wang, D. C. Baars, T. R. Bieler, S. N. Mathaudhu, and R. E. Barber, IEEE Trans. Appl. Supercond. **17**, 1305 (2007).
[26] C. W. Chen, *Magnetism and Metallurgy of Soft Magnetic Materials*, Selected Topics in Solid State Physics, edited by E. P. Wohlfarth (North-Holland, Amsterdam, 1977), Vol. XV, pp. 299–308.
[27] J. T. Park and J. A. Szpunar, Acta Mater. **51**, 3037 (2003).
[28] M. F. de Campos, F. J. G. Landgraf, I. G. S. Falleiros, G. C. Fronzaglia, and H. Kahn, ISIJ International **44**, 1733 (2004).
[29] M. Kothari and L. Anand, J. Mech. Phys. Solids **46**, 51 (1998).
[30] M. A. Meyers, D. J. Benson, O. Vohringer, B. K. Kad, Q. Xue, and H. H. Fu, Mater. Sci. Eng. A **322**, 194 (2002).
[31] L. Stainier, A. M. Cuitino, and M. Ortiz, J. Phys. IV **105**, 157 (2003).
[32] A. Ma, F. Roters, and D. Raabe, Comput. Mater. Sci. **39**, 91 (2007).
[33] A. Zamiri, H. Jiang, T. R. Bieler, and F. Pourboghrat, JOM **60**, 70 (2008).
[34] A. Zamiri and F. Pourboghrat, Int. J. Solids Struct. **44**, 8627 (2007).
[35] D. Baars, H. Jiang, T. R. Bieler, A. Zamiri, F. Pourboghrat, and C. Compton, *Applications of Texture Analysis: Ceramic Transactions* (Wiley, New York, 2008), Vol. 201, p. 391.
[36] R. D. Doherty, D. A. Hughes, F. J. Humphreys, J. J. Jonas, D. Juul Jensen, M. E. Kassner, W. E. King, T. R. McNelley, H. J. McQueen, and A. D. Rollet, Mater. Sci. Eng. A **238**, 219 (1997).
[37] T. Kumano, T. Haratani, and Y. Ushigami, ISIJ International **42**, 440 (2002).
[38] D. A. Molodov, U. Czubayko, G. Gottstein, and L. S. Shvindlerman, Acta Mater. **46**, 553 (1998).
[39] H. Padamsee, J. Knobloch, and T. Hays, *RF Superconductivity for Accelerators* (Wiley-VCH, New York, 2008), 2nd ed.
[40] H. Jiang, T. R. Bieler, C. Compton, and T. Grimm, in *Proceedings of the 20th Particle Accelerator Conference, Portland, OR, 2003* (IEEE, New York, 2003), pp. 1359–1361.
[41] R. Komanduri and Z. B. Hou, Metall. Mater. Trans. B **32**, 483 (2001).
[42] A. Romanenko, Crystalline Microstructure Role in the High Field Q-Slope, SRF2009, Berlin, Germany, SRF2009 WEB Proceedings, paper TUOAAU02, pp. 95–101, ISSN 1868-5781.
[43] X. Zhao, G. Ciovati, C. E. Reece, and A. T. Wu, Study of Etching Pits in a Large-Grain Single Cell Bulk Niobium Cavity, SRF2009, Berlin, Germany, SRF2009 WEB Proceedings, paper TUPPO087, pp. 446–49, ISSN 1868-5781.
[44] E. F. Cotts, D. M. Miliotis, and A. C. Anderson, Phys. Rev. B **24**, 7336 (1981).
[45] W. Singer, A. Brinkmann, A. Ermakov, J. Iversen, G. Kreps, A. Matheisen, D. Proch, D. Reschke, X. Singer, M. Spiwek, H. Wen, and H. -G. Brokmeier, AIP Conf. Proc. **927**, 123 (2007).